

Ultrafast Unbalanced Electron Distributions in Quasicrystalline 30° Twisted Bilayer Graphene

Takeshi Suzuki,^{*,†} Takushi Iimori,[†] Sung Joon Ahn,[‡] Yuhao Zhao,[†] Mari Watanabe,[†] Jiadi Xu,[†] Masami Fujisawa,[†] Teruto Kanai,[†] Nobuhisa Ishii,[†] Jiro Itatani,[†] Kento Suwa,[§] Hirokazu Fukidome,[§] Satoru Tanaka,[⊥] Joung Real Ahn,^{‡,||} Kozo Okazaki,^{†,#} Shik Shin,^{†,#,¶} Fumio Komori,^{*,†} and Iwao Matsuda^{*,†}

[†]Institute for Solid State Physics, The University of Tokyo, Kashiwa, Chiba 277-8581, Japan

[‡]Department of Physics and SAINT, Sungkyunkwan University, Suwon, Gyeonggi-do 16419, Republic of Korea

[§]Research Institute of Electrical Communication, Tohoku University, Sendai, Miyagi 980-8577, Japan

[⊥]Department of Applied Quantum Physics and Nuclear Engineering, Kyushu University, Fukuoka, Fukuoka 819-0395, Japan

^{||}Samsung-SKKU Graphene Centre, Sungkyunkwan University, Suwon, Gyeonggi-do 440-746, Republic of Korea

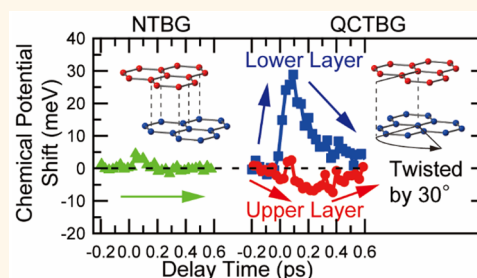
[#]OPERANDO-OIL, AIST, Kashiwa, Chiba 277-8581, Japan

[¶]The University of Tokyo, Kashiwa, Chiba 277-8581, Japan

Supporting Information

ABSTRACT: Ultrafast carrier dynamics in a graphene system are very important in terms of optoelectronic devices. Recently, a twisted bilayer graphene has been discovered that possesses interesting electronic properties owing to strong modifications in interlayer couplings. Thus, a better understanding of ultrafast carrier dynamics in a twisted bilayer graphene is highly desired. Here, we reveal the unbalanced electron distributions in a quasicrystalline 30° twisted bilayer graphene (QCTBG), using time- and angle-resolved photoemission spectroscopy on the femtosecond time scale. We distinguish time-dependent electronic behavior between the upper- and lower-layer Dirac cones and gain insight into the dynamical properties of replica bands, which show characteristic signatures due to Umklapp scatterings. The experimental results are reproduced by solving a set of rate equations among the graphene layers and substrate. We find that the substrate buffer layer plays a key role in initial carrier injections to the upper and lower layers. Our results demonstrate that QCTBG can be a promising element for future devices.

KEYWORDS: graphene, interfaces, quasicrystal, valleytronics, ultrafast dynamics, and optoelectronics



Layers of twisted bilayer graphene exhibit varieties of exotic quantum phenomena.^{1–5} Currently, the twist angle Θ has become an important degree of freedom for investigating many interesting states of matter, that is, two-dimensional superconductivity ($\Theta = 1.1^\circ$)^{6,7} and a two-dimensional quasicrystal ($\Theta = 30^\circ$).^{8,9} We report herein experimental observations of the photoinduced ultrafast dynamics of Dirac Fermions in a quasicrystalline 30° twisted bilayer graphene (QCTBG). Using time- and angle-resolved photoemission spectroscopy, we discover that hot carriers are asymmetrically distributed between the two graphene layers, followed by the opposing femtosecond relaxations. The key mechanism of asymmetric carrier distributions involves the differing carrier transport between layers and the transient doping from the substrate interface. The ultrafast dynamics scheme continues after Umklapp scattering, which is induced by the incommensurate interlayer stacking of the quasi-

crystallinity. The dynamics in the atomic layer demonstrates great potential of QCTBG for future application and creates interdisciplinary links in the optoelectronics of van der Waals crystals.

Carrier dynamics in graphene is determined by Fermions in a linearly dispersing band structure, the Dirac cones, which have successfully offered exciting electronic properties in terms of transport and optics and achieved many applications.¹⁰ Nonequilibrium electronic states in matter, generated by optical pumping, are characterized by the transient temperature. In an *n*-type graphene layer (Figure 1a) typically produced on a SiC substrate over a large area, the temporal chemical potential reduces with the temperature, as shown in

Received: August 1, 2019

Accepted: September 25, 2019

Published: September 25, 2019

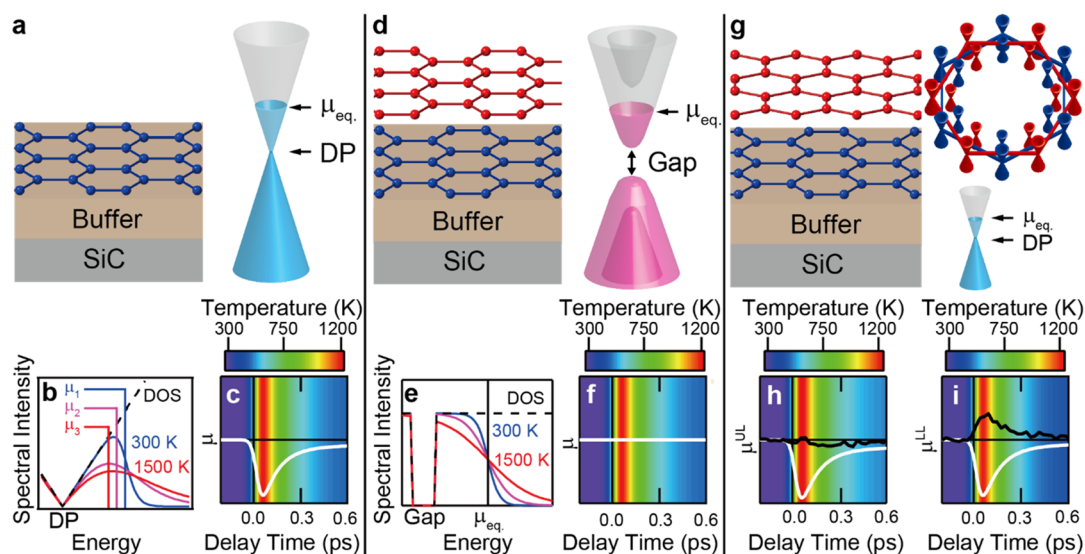


Figure 1. Crystal and electronic structures of *n*-type single-layer, bilayer, and quasicrystalline 30° twisted bilayer graphenes (QCTBGs) and hot carrier dynamics. (a) Crystal and electronic structure of single-layer graphene. Dirac point and equilibrium chemical potential are denoted as DP and μ_{eq} , respectively. (b) Spectral intensities with different temperatures for single-layer graphene. (c) Dynamics of temperature and chemical potential shifts for hot carriers. (d) Crystal and electronic structure of bilayer graphene. (e) Spectral intensities with different temperatures for bilayer graphene. (f) Dynamics of temperature and chemical potential shifts for hot carriers. (g) Crystal and electronic structure of QCTBG. Outer red and blue Dirac cones represent the ULD and LLD bands, respectively, whereas the inner red and blue Dirac cones correspond to the replica bands of the ULD and LLD bands. (h,i) Dynamics of temperature and chemical potential shifts for hot carriers in the ULD and LLD bands. Experimental data of chemical potential shifts are shown as black solid lines for the ULD (h) and LLD (i) bands, respectively.

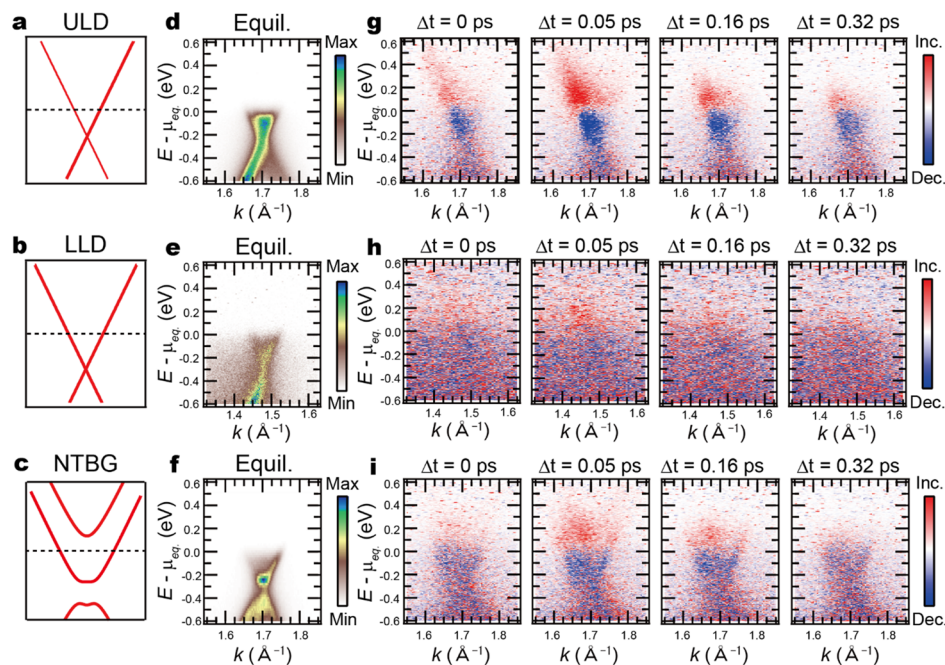


Figure 2. TARPES spectra for QCTBG and nontwisted bilayer graphene. (a–c) Calculated band structures for the ULD and LLD bands in QCTBG and the nontwisted bilayer graphene (NTBG) band, respectively. Dashed lines indicate the Fermi level. (d–f) Equilibrium angle-resolved photoemission spectra for the ULD, LLD, and NTBG bands. (g–i) Difference images of time- and angle-resolved photoemission spectroscopy (TARPES) for the ULD, LLD, and NTBG bands. Red and blue points represent increasing and decreasing photoemission intensity, respectively.

Figure 1b,c. This dynamical phenomenon is specific to the massless Dirac Fermion and is caused by keeping the charge-neutrality conditions in the linear density of states (DOS). In contrast, an *n*-type bilayer graphene, shown in **Figure 1d**, on a substrate has massive Fermions with an energy gap that is

formed by an interband interaction of Dirac states between the two layers. The DOS becomes constant and, thus, the position of the chemical potential does not depend on the temperature (**Figure 1e,f**). For the QCTBG, the interlayer interaction is minimal because of the 30° twisted angle and the massless

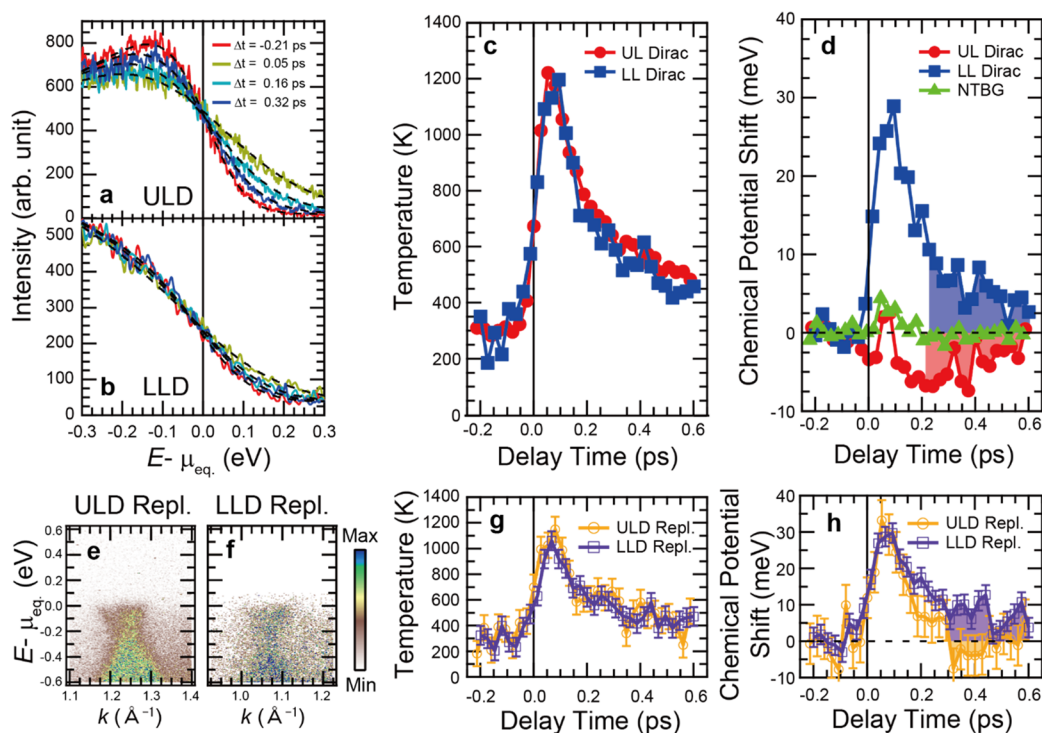


Figure 3. Time-dependence of electronic temperature and chemical-potential shift. (a,b) Energy-distribution curves for the ULD and LLD bands as a function of pump–probe delays Δt , respectively. Dashed lines are fits to Fermi–Dirac distribution curves. (c) Electronic temperature as a function of pump–probe delay time for the ULD and LLD bands. (d) Chemical-potential shift as a function of pump–probe delay time for the ULD and LLD bands. For comparison, the result for NTBG is also shown. (e,f) Equilibrium angle-resolved photoemission spectroscopy map for replicas of the ULD and LLD bands. (g,h) Electronic temperatures and chemical-potential shift as a function of pump–probe delay time for the replicas of the ULD and LLD bands. Errors are estimated from the standard deviation in the data before the arrival of the pump pulse.

Dirac Fermions remain in the two layers. As shown in Figure 1g, the electronic state results in a 12-fold (dodecagonal) structure, which is composed of upper-layer Dirac (ULD) and lower-layer Dirac (LLD) cones, with their replicas formed because of the strong interlayer coupling that connects the Umklapp scattering in each layer (Figure S1). The QCTBG doubles the two-dimensional number density of Dirac Fermions that follows the carrier dynamics in Figure 1b,c. Here, we discover that the transient chemical potential is distinctive and that it actually shows contrasting behavior between the ULDs and LLDs, as shown in Figure 1h,i, whereas each Dirac Fermion follows the carrier dynamics in Figure 1b,c. The main objective of this work is to share our observations of these striking phenomena in the dynamics of the QCTBG and to provide a possible origin of the contrasting ultrafast behavior.

The electronic structure of QCTBG makes it ideal for investigating physical properties relying on quasi-crystallinity that may lead to many applications of electronics and optics in graphene technology. We explore this electronic structure by focusing on the ultrafast dynamics on the femtosecond time scale through time- and angle-resolved photoemission spectroscopy (TARPES), which allows us to directly observe the temporal evolution of Fermions in the Dirac cones (see Figure 1c). TARPES has already revealed dynamical events, such as the bottleneck effect^{11,12} and the supercollision process,^{13,14} which are specific to Dirac Fermions in single-layer graphene. Thus, we apply TARPES to the quasi-periodic graphene system and compare the results with those of a periodic graphene system. The measurement used the pump–probe

approach with an infrared pulse with $h\nu = 1.55$ eV serving as the pump and an extreme-ultraviolet pulse with $h\nu = 21.7$ eV serving as the probe to cover the entire 2D Brillouin zone (Figure S2c).

RESULTS AND DISCUSSION

Time- and Angle-Resolved Photoemission Spectroscopy. Figure 2 summarizes the time-resolved photoemission band diagrams acquired at selected delay times for the ULD and LLD bands in QCTBG. By rotating the sample about the slit of the analyzer, we can tune the detecting position in the momentum space and selectively observe the ULD and LLD bands. The results for periodic nontwisted bilayer graphene (NTBG) are also shown for comparison. The measured spectra are consistent with the calculated band structure (Figure 2a–f). The Dirac cones of QCTBG are *n*-type at the Dirac points, where Dirac points are below the equilibrium chemical potential (μ_{eq}). The electronic structure of NTBG is also *n*-type and there is a band gap around μ_{eq} (Figure S3).^{15,16} After the pump pulse (intensity ~ 0.7 mJ/cm²), the TARPES band diagram of individual bands of bilayers evolves on the femtosecond time scale. To enhance the temporal variations, the band diagrams are shown as the difference between the spectra before and after photoexcitation, where red and blue in Figure 2g–i represent an increase and decrease in photoemission intensity, respectively. The spectral weights for all bands decrease immediately below μ_{eq} and increase above μ_{eq} at $\Delta t = 0.05$ ps. This reflects the excitation of electrons from the occupied bands to the unoccupied bands. At $\Delta t = 0.16$ and

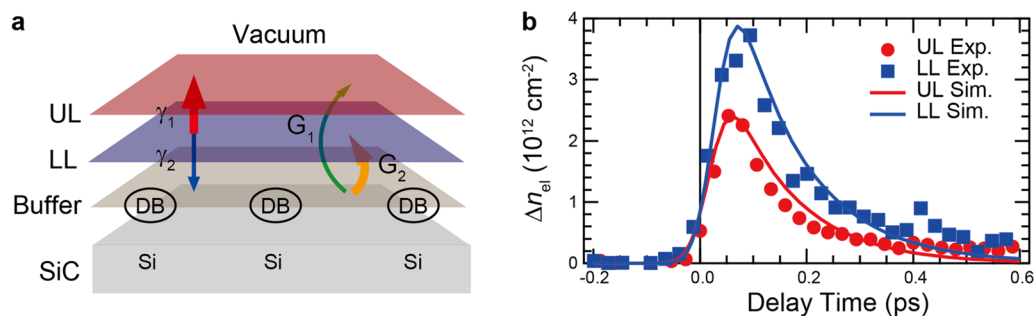


Figure 4. Carrier transport among layers in QCTBG. (a) Schematic illustration of the spatial relationships among the upper layer (UL), lower layer (LL), buffer layer, and SiC substrate in QCTBG. Schematic illustration of carrier transport among layers in QCTBG are shown by arrows. γ_1 and γ_2 are rate constants of carrier transfer between the UL and LL, and the LL and SiC substrate, respectively. G_1 and G_2 are coefficients of pump-induced net density flux to the UL and LL from the SiC substrate, respectively. Thicker lines indicate the larger values of γ_1 than γ_2 and G_2 than G_1 . (b) Time-dependent total electron densities, Δn_{el} , for the UL and LL. Experimental results are shown as symbols whereas calculation results by solving rate equations are shown as lines.

0.32 ps, the difference intensity decreases with delay time, which corresponds to the relaxation of photoexcited carriers.

To evaluate the occupation of Dirac cones by non-equilibrium carriers, we plot energy distribution curves of the Dirac bands by integrating photoemission intensities over momentum space. Figure 3a,b shows a series of energy distribution curves for the UL and LLD bands, respectively, for several pump–probe delay times Δt . The spectra are fit by the Fermi–Dirac distribution function convoluted by a Gaussian to extract the electronic temperature (Figure 3c) and chemical-potential shift $\Delta\mu$ (Figure 3d) for the UL and LLD bands. The similar time evolution for temperature in Figure 3c indicates that photoexcited carriers in the two bands take the same relaxation pathway. In contrast, the different time evolution for $\Delta\mu$ indicates that the UL and LLD bands display opposite behavior after $\Delta t = 0.2$ ps (i.e., the UL undergoes a negative shift whereas the LLD undergoes a positive shift). Interestingly, $\Delta\mu$ for the NTBG band remains constant at essentially zero over the same time delay. The striking difference among the three types of Dirac cones provides clear evidence of a carrier imbalance between the UL and LLD bands of the QCTBG on the ultrafast time scale.

We now discuss the UL and LLD replica band TARPES results. Figure 3g,h shows the time dependence of temperature and $\Delta\mu$, respectively. For the transient temperature, the temporal profiles of the replica bands are almost identical to each other and to those of the original bands (Figure S4), which indicates that during relaxation photoexcited electrons occupying Dirac cones interact via electron–phonon interactions with the common phonon bath. The nonequilibrium chemical potential $\Delta\mu$ of the LLD replica band is positive and decreases monotonically, as it does for the original LLD band. In contrast, $\Delta\mu$ for the UL replica band is initially positive and then becomes slightly negative and approaches zero when $\Delta t > 0.3$ ps. The sign inversion of the UL replica band differs significantly from the dynamics of the original UL band, which implies that the electron distribution between the replica Dirac cones and the original Dirac cones is also unbalanced.

Rate Equations. In general, the temperature increases and $\Delta\mu$ is negative for *n*-type graphene after photoexcitation, as reported previously.¹⁷ Thus, the temporal evolution of the UL (replica) band is natural. Conversely, the positive $\Delta\mu$ of the LLD (replica) band is quite striking. As previously mentioned, the chemical potential is determined by temper-

ature and carrier density for Dirac Fermions. Thus, the observed difference in chemical potentials stems from the asymmetric carrier transport between the upper layer (UL) and lower layer (LL). To gain quantitative insight, we perform calculations by solving rate equations for carrier transport. The spatial relation of the UL, LL, and SiC substrate and coefficients of carrier transfers used in the following set of rate equations are shown in Figure 4a

$$\frac{dn_{\text{el}}^{\text{UL}}}{dt} = -\frac{n_{\text{el}}^{\text{UL}}}{\tau_{\text{UL}}} + \gamma_1(n_{\text{el}}^{\text{LL}} - n_{\text{el}}^{\text{UL}}) + G_1 \exp\left(-\frac{t^2}{T_p^2}\right) \quad (1)$$

$$\frac{dn_{\text{el}}^{\text{LL}}}{dt} = -\frac{n_{\text{el}}^{\text{LL}}}{\tau_{\text{LL}}} - \gamma_1(n_{\text{el}}^{\text{LL}} - n_{\text{el}}^{\text{UL}}) - \gamma_2(n_{\text{el}}^{\text{LL}} - n_{\text{el}}^{\text{Sub}}) + G_2 \exp\left(-\frac{t^2}{T_p^2}\right) \quad (2)$$

$$n_{\text{el}}^{\text{UL}} + n_{\text{el}}^{\text{LL}} + n_{\text{el}}^{\text{Sub}} = \text{const} \quad (3)$$

where $n_{\text{el}}^{\text{UL/LL}}$ and $\tau_{\text{UL/LL}}$ are electron densities and lifetimes in the UL/LLD band of a QCTBG, respectively. γ_1 and γ_2 are rate constants of carrier transfer between the UL and LL, and the LL and SiC substrate. G_1 and G_2 are coefficients of pump-induced net density flux to the UL and LL from the SiC substrate, respectively. T_p is the time width, reflecting the temporal resolution. $n_{\text{el}}^{\text{Sub}}$ is the electron density in the SiC substrate, and eq 3 corresponds to the carrier conservation. The detailed procedure to solve the rate equations is shown in the Supporting Information.

The change of total electron densities, Δn_{el} , for the UL and LL can be extracted from both the time-dependent electron temperature and chemical potential (Figure 3c,d), shown as markers in Figure 4b. To reproduce the best agreement with the experiments, we set $\gamma_1 = 1.5 \text{ ps}^{-1}$, $\gamma_2 = 0.5 \text{ ps}^{-1}$, $G_1 = 5 \times 10^{13} \text{ cm}^{-2} \text{ ps}^{-1}$, and $G_2 = 8 \times 10^{13} \text{ cm}^{-2} \text{ ps}^{-1}$, and calculation results are shown as solid lines in Figure 4b.

The carrier transferring rates are shown as widths of arrows in Figure 4a. We find that the experimental results are reproduced when the γ_1 value is larger than γ_2 , indicating that carrier transfer is much more frequent between graphene layers than between the LL and substrate. Most importantly, the apparent G_1 and G_2 values demonstrate there is transient carrier doping from the substrate to the graphene layers. The unexpected carrier imbalance, shown in Figure 4b, seems to be due to differing values between G_1 and G_2 , which determine the initial electron distributions in the UL and LL. It is of note

that the larger G_2 value is consistent with the closer distance of the LL to the substrate. Origins of the external flux in the graphene layers can be explained as due to electrons in the Si dangling-bond (DB) state at the graphene/SiC interface.¹⁸ A possibility of creating the photoexcited carriers in a SiC crystal is excluded as the pumping photon energy ($h\nu = 1.55$ eV) is not high enough to overcome the SiC bulk band gap (3.3 eV). The DB bands have been known to exist at the Fermi level that is located almost at the bottom of the SiC conduction band.¹⁸ The area density of Si DBs at the interface corresponds to the order of 10^{15} cm⁻², whereas the density of states in single-layer graphene is only in the order of 10^{12} – 10^{13} cm⁻² near the Dirac point.¹⁹ As a number of electrons in the Si DBs (interface states) are several orders of magnitude higher than that of the graphene density of states, carrier doping to the UL and LL can be large enough to dominate the transient chemical potential.

Umklapp Scattering and Unbalanced Carrier Distributions. In electronic transport, Umklapp scattering plays an intrinsically central role in increasing the resistivity at low temperature, although other effects often hinder its clear identification.²⁰ Recent technological advances in graphene devices have led to superlattices with small lattice mismatch in which electron–electron Umklapp scattering is clearly demonstrated.²¹ By inducing strong interlayer coupling, QCTBG can be regarded as an alternative route to study Umklapp scattering.^{8,9} In this respect, studying carrier dynamics by using ultrafast optical spectroscopy can complement transport studies of a twisted bilayer graphene,²² and important evidence is provided by the strong correlation between the dynamic properties of the original and replica bands of QCTBG as previously discussed and shown in Figure 3e–h.

The unbalanced electron distributions in the ULD and LLD bands discovered in the present study present an additional functionality that can be advantageous in optoelectronic applications using graphene. The key mechanism here is the difference in carrier transfer between the two graphene layers, which is controllable by band engineering, for example, by doping¹⁵ or intercalation^{23,24} in NTB. In terms of applications, the transient population inversion can be augmented by using excess electron transfer from the ULD band to the LLD band. The energy scale of the observed chemical potential shift is ~ 10 meV, so one can anticipate a lasing medium operating in the terahertz range, which is of technological interest.^{25,26} In the field of excitonic physics in bilayer graphene,²⁷ asymmetric electron and hole distributions between the upper and lower layers lead to spatially separated interlayer excitons. By twisting the two layers, the electrons and holes can be separated in momentum space and in real space, as reported for the van der Waals heterostructure.²⁸ This will allow us to investigate valleytronics in bilayer graphene.

CONCLUSIONS

We have studied the ultrafast carrier dynamics of QCTBG by using TARPES. We have successfully distinguished the carrier dynamics between the upper- and lower-layer Dirac cones as well as replica bands of them. From the analysis of EDC curves, we have found that the electron distributions between the upper and lower layers were unbalanced, which was well explained by performing calculations based on rate equations. The present investigations demonstrate the feasibility of manipulating the dynamics of Dirac carriers in individual

layers of bilayer graphene and provide valuable information for designing future graphene-based ultrafast optoelectronic devices.

MATERIALS AND METHOD

Sample Preparation. The QCTBG was grown on the Si face of a 4H-SiC (0001) substrate by thermal decomposition of the substrate in a vacuum after growing a monatomic hexagonal boron nitride layer. The upper and lower layers were rotated by 0° and 30° with respect to the orientation of the SiC (0001) surface. Details of the growth procedure have been previously reported.⁸ The NTB was grown on the Si-face of a vicinal 6H-SiC substrate by thermal decomposition in a vacuum.²⁹ After transferring through air to an ultrahigh-vacuum chamber, the graphene was cleaned by annealing at 450 °C to remove surface contamination.

Photoemission Measurement. To characterize the sample, static angle-resolved photoemission spectroscopy measurements were made using a He discharge lamp and a hemispherical electron analyzer (Omicron-Scienta R4000) with an energy resolution of ~ 12.5 meV. For the TARPES measurements, we used a commercial Ti:sapphire regenerative amplifier system (Spectra-Physics, Solstice Ace) with a center wavelength of 800 nm and pulse width of ~ 35 fs for the pump pulse. Second harmonic pulses generated in a 0.2 mm thick crystal of β -BaB₂O₄ were focused into a static gas cell filled with Ar to generate higher harmonics. By using a set of SiC/Mg multilayer mirrors, we selected the seventh harmonic of the second harmonic ($h\nu = 21.7$ eV) for the probe pulse. The temporal resolution was determined to be ~ 70 fs from the TARPES intensity more than 0.6 eV above the Fermi level, corresponding to the cross correlation between the pump and probe pulses.

Analysis of Experimental Data. The energy distribution curves for each band were analyzed by fitting a Fermi–Dirac distribution convoluted with a Gaussian such that the density of states, Gaussian width, and background remain fixed while the electronic temperature and chemical potential are varied to obtain the best fit. As we fixed the parameters for background, the temperature and chemical potentials were not affected by the background signal. Errors were estimated based on the standard deviation of the fitting parameters well before the arrival of the pump pulse.

Rate Equations. The details of the rate equation solution are shown in the Supporting Information.

ASSOCIATED CONTENT

Supporting Information

The Supporting Information is available free of charge on the ACS Publications website at DOI: 10.1021/acsnano.9b06091.

Umklapp scattering and replica bands, crystal and electronic structures for quasicrystalline 30° twisted bilayer graphene and experimental setup, model and calculation for nontwisted bilayer graphene, evaluation of time constant of time-dependent electronic temperature for each band in QCTBG, simulation results of rate equations (PDF)

AUTHOR INFORMATION

Corresponding Authors

*E-mail: takeshi.suzuki@issp.u-tokyo.ac.jp.

*E-mail: komori@issp.u-tokyo.ac.jp.

*E-mail: imatsuda@issp.u-tokyo.ac.jp.

ORCID

Takeshi Suzuki: 0000-0003-1261-7131

Joung Real Ahn: 0000-0003-4300-4741

Fumio Komori: 0000-0002-6405-4177

Iwao Matsuda: 0000-0002-2118-9303

Author Contributions

T.S., T.I., Z.Y., M.W., and J.X. carried out the TARPES measurements. T.S. analyzed the data. T.S. and I.M. performed the calculations. M.F., T.K., N.L., and J.I. maintained the HHG laser system and improved the TARPES apparatus. K.S., H.F., and S.T. grew the high-quality nontwisted bilayer graphene. S.J.A. and J.R.A. grew the high-quality QCTBG and characterized it. T.S., K.O., S.S., F.K., and I.M. wrote the manuscript. K.O., S.S., F.K., and I.M. designed the project. All authors discussed the results and contributed to the manuscript.

Notes

The authors declare no competing financial interest.

ACKNOWLEDGMENTS

We would like to acknowledge Y. Tsujikawa, M. Sakamoto, and A. Takayama for their kind support during the experiments. We would also like to thank M. Koshino, T. Ishimasa, K. Kimura, and E. Minamitani for valuable discussions and comments. This work was supported by Grants-in-Aid for Scientific Research (KAKENHI) (Grants 16H06361, 18H03874, 18K19011, 18K13498, 18H01146, 19H00659, 19H01818, and 19H00651) from Japan Society for the Promotion of Science (JSPS) and by JSPS KAKENHI on Innovative Areas “Quantum Liquid Crystals” (Grant 19H05826), and by Quantum Leap Flagship Program (Q-LEAP) (Grant JPMXS0118068681) from the Ministry of Education, Culture, Sports, Science, and Technology (MEXT).

REFERENCES

- (1) Ponomarenko, L. A.; Gorbachev, R. V.; Yu, G. L.; Elias, D. C.; Jalil, R.; Patel, A. A.; Mishchenko, A.; Mayorov, A. S.; Woods, C. R.; Wallbank, J. R.; Mucha-Kruczynski, M.; Piot, B. A.; Potemski, M.; Grigorieva, I. V.; Novoselov, K. S.; Guinea, F.; Fal'ko, V. I.; Geim, A. K. Cloning of Dirac Fermions in Graphene Superlattices. *Nature* **2013**, *497*, 594–597.
- (2) Dean, C. R.; Wang, L.; Maher, P.; Forsythe, C.; Ghahari, F.; Gao, Y.; Katoch, J.; Ishigami, M.; Moon, P.; Koshino, M.; Taniguchi, T.; Watanabe, K.; Shepard, K. L.; Hone, J.; Kim, P. Hofstadter's Butterfly and the Fractal Quantum Hall Effect in Moiré Superlattices. *Nature* **2013**, *497*, 598–602.
- (3) Hunt, B.; Sanchez-Yamagishi, J. D.; Young, A. F.; Yankowitz, M.; LeRoy, B. J.; Watanabe, K.; Taniguchi, T.; Moon, P.; Koshino, M.; Jarillo-Herrero, P.; Ashoori, R. C. Massive Dirac Fermions and Hofstadter Butterfly in a van der Waals Heterostructure. *Science* **2013**, *340*, 1427–1430.
- (4) Gorbachev, R. V.; Song, J. C. W.; Yu, G. L.; Kretinin, A. V.; Withers, F.; Cao, Y.; Mishchenko, A.; Grigorieva, I. V.; Novoselov, K. S.; Levitov, L. S.; Geim, A. K. Detecting Topological Currents in Graphene Superlattices. *Science* **2014**, *346*, 448–451.
- (5) Zhu, M.; Ghazaryan, D.; Son, S.-K.; Woods, C. R.; Misra, A.; He, L.; Taniguchi, T.; Watanabe, K.; Novoselov, K. S.; Cao, Y.; Mishchenko, A. Stacking Transition in Bilayer Graphene Caused by Thermally Activated Rotation. *2D Mater.* **2017**, *4*, No. 011013.
- (6) Cao, Y.; Fatemi, V.; Fang, S.; Watanabe, K.; Taniguchi, T.; Kaxiras, E.; Jarillo-Herrero, P. Unconventional Superconductivity in Magic-Angle Graphene Superlattices. *Nature* **2018**, *556*, 43–50.
- (7) Cao, Y.; Fatemi, V.; Demir, A.; Fang, S.; Tomarken, S. L.; Luo, J. Y.; Sanchez-Yamagishi, J. D.; Watanabe, K.; Taniguchi, T.; Kaxiras, E.; Ashoori, R. C.; Jarillo-Herrero, P. Correlated Insulator Behaviour at Half-Filling in Magic-Angle Graphene Superlattices. *Nature* **2018**, *556*, 80–84.
- (8) Ahn, S. J.; Moon, P.; Kim, T.-H.; Kim, H.-W.; Shin, H.-C.; Kim, E. H.; Cha, H. W.; Kahng, S.-J.; Kim, P.; Koshino, M.; Son, Y.-W.; Yang, C.-W.; Ahn, J. R. Dirac Electrons in a Dodecagonal Graphene Quasicrystal. *Science* **2018**, *361*, 782–786.
- (9) Yao, W.; Wang, E.; Bao, C.; Zhang, Y.; Zhang, K.; Bao, K.; Chan, C. K.; Chen, C.; Avila, J. M.; Asensio, C.; Zhu, J.; Zhou, S. Quasicrystalline 30° Twisted Bilayer Graphene as an Incommensurate Superlattice with Strong Interlayer Coupling. *Proc. Natl. Acad. Sci. U. S. A.* **2018**, *115*, 6928.
- (10) Castro Neto, A. H.; Guinea, F.; Peres, N. M. R.; Novoselov, K. S.; Geim, A. K. The Electronic Properties of Graphene. *Rev. Mod. Phys.* **2009**, *81*, 109–162.
- (11) Gierz, I.; Petersen, J. C.; Mitrano, M.; Cacho, C.; Turcu, I. C. E.; Springate, E.; Stöhr, A.; Köhler, A.; Starke, U.; Cavalleri, A. Snapshots of Non-Equilibrium Dirac carrier Distributions in Graphene. *Nat. Mater.* **2013**, *12*, 1119–1124.
- (12) Ulstrup, S.; Johannsen, J. C.; Cilento, F.; Miwa, J. A.; Crepaldi, A.; Zacchigna, M.; Cacho, C.; Chapman, R.; Springate, E.; Mammadov, S.; Fromm, F.; Raidel, C.; Seyller, T.; Parmigiani, F.; Grioni, M.; King, P. D. C.; Hofmann, P. Ultrafast Dynamics of Massive Dirac Fermions in Bilayer Graphene. *Phys. Rev. Lett.* **2014**, *112*, 257401.
- (13) Johannsen, J. C.; Ulstrup, S.; Cilento, F.; Crepaldi, A.; Zacchigna, M.; Cacho, C.; Turcu, I. C. E.; Springate, E.; Fromm, F.; Raidel, C.; Seyller, T.; Parmigiani, F.; Grioni, M.; Hofmann, P. Direct View of Hot Carrier Dynamics in Graphene. *Phys. Rev. Lett.* **2013**, *111*, No. 027403.
- (14) Someya, T.; Fukidome, H.; Watanabe, H.; Yamamoto, T.; Okada, M.; Suzuki, H.; Ogawa, Y.; Iimori, T.; Ishii, N.; Kanai, T.; Tashima, K.; Feng, B.; Yamamoto, S.; Itatani, J.; Komori, F.; Okazaki, K.; Shin, S.; Matsuda, I. Suppression of Supercollision Carrier Cooling in High Mobility Graphene on SiC(0001). *Phys. Rev. B: Condens. Matter Mater. Phys.* **2017**, *95*, 165303.
- (15) Ohta, T.; Bostwick, A.; Seyller, T.; Horn, K.; Rotenberg, E. Controlling the Electronic Structure of Bilayer Graphene. *Science* **2006**, *313*, 951–954.
- (16) Marchenko, D.; Evtushinsky, D. V.; Golias, E.; Varykhalov, A.; Seyller, Th.; Rader, O. Extremely Flat Band in Bilayer Graphene. *Sci. Adv.* **2018**, *4*, No. eaau0059.
- (17) Someya, T.; Fukidome, H.; Ishida, Y.; Yoshida, R.; Iimori, T.; Yukawa, R.; Akikubo, K.; Yamamoto, Sh.; Yamamoto, S.; Yamamoto, T.; Kanai, T.; Funakubo, K.; Suemitsu, M.; Itatani, J.; Komori, F.; Shin, S.; Matsuda, I. Observing Hot Carrier Distribution in an N-Type Epitaxial Graphene on a SiC Substrate. *Appl. Phys. Lett.* **2014**, *104*, 161103.
- (18) Kajihara, M.; Suzuki, T.; Shahed, S. M. F.; Komeda, T.; Minamitani, E.; Watanabe, S. DFT Calculations on Atom-Specific Electronic Properties of G/SiC(0001). *Surf. Sci.* **2016**, *647*, 39–44.
- (19) Someya, T.; Fukidome, H.; Endo, N.; Takahashi, K.; Yamamoto, S.; Matsuda, I. Interfacial Carrier Dynamics of Graphene on SiC, Traced by the Full-Range Time-Resolved Core-Level Photoemission Spectroscopy. *Appl. Phys. Lett.* **2018**, *113*, No. 051601.
- (20) Bass, J.; Pratt, W. P.; Schroeder, P. A. The Temperature-Dependent Electrical Resistivities of the Alkali Metals. *Rev. Mod. Phys.* **1990**, *62*, 645–744.
- (21) Wallbank, J. R.; Krishna, K. R.; Holwill, M.; Wang, Z.; Auton, G. H.; Birkbeck, J.; Mishchenko, A.; Ponomarenko, L. A.; Watanabe, K.; Taniguchi, T.; Novoselov, K. S.; Aleiner, I. L.; Geim, A. K.; Fal'ko, V. I. Excess Resistivity in Graphene Superlattices Caused by Umklapp Electron-Electron Scattering. *Nat. Phys.* **2019**, *15*, 32–36.
- (22) Kim, Y.; Yun, H.; Nam, S.-G.; Son, M.; Lee, D. S.; Kim, D. C.; Seo, S.; Choi, H. C.; Lee, H.-J.; Lee, S. W.; Kim, J. S. Breakdown of the Interlayer Coherence in Twisted Bilayer Graphene. *Phys. Rev. Lett.* **2013**, *110*, No. 096602.
- (23) Zhou, S. Y.; Siegel, D. A.; Fedorov, A. V.; Lanzara, A. Metal to Insulator Transition in Epitaxial Graphene Induced by Molecular Doping. *Phys. Rev. Lett.* **2008**, *101*, No. 086402.
- (24) Riedl, C.; Coletti, C.; Iwasaki, T.; Zakharov, A. A.; Starke, U. Quasi-Free-Standing Epitaxial Graphene on SiC Obtained by Hydrogen Intercalation. *Phys. Rev. Lett.* **2009**, *103*, 246804.
- (25) Wang, F.; Zhang, Y.; Tian, C.; Girit, C.; Zettl, A.; Crommie, M.; Shen, T. R. Gate-Variable Optical Transitions in Graphene. *Science* **2008**, *320*, 206–209.

(26) Kar, S.; Nguyen, V. L.; Mohapatra, D. R.; Lee, Y. H.; Sood, A. K. Ultrafast Spectral Photoresponse of Bilayer Graphene: Optical Pump-Terahertz Probe Spectroscopy. *ACS Nano* **2018**, *12*, 1785–1792.

(27) Ju, L.; Wang, L.; Cao, T.; Taniguchi, T.; Watanabe, K.; Louie, S. G.; Rana, F.; Park, J.; Hone, J.; Wang, F.; McEuen, P. L. Tunable Excitons in Bilayer Graphene. *Science* **2017**, *358*, 907–910.

(28) Kunstmann, J.; Mooshammer, F.; Nagler, P.; Chaves, A.; Stein, F.; Paradiso, N.; Plechinger, G.; Strunk, C.; Schüller, C.; Seifert, G.; Reichman, D. R.; Korn, T. Momentum-Space Indirect Interlayer Excitons in Transition-Metal Dichalcogenide van der Waals Heterostructures. *Nat. Phys.* **2018**, *14*, 801–805.

(29) Tanaka, S.; Morita, K.; Hibino, H. Anisotropic Layer-by-Layer Growth of Graphene on Vicinal SiC(0001) Surfaces. *Phys. Rev. B: Condens. Matter Mater. Phys.* **2010**, *81*, No. 041406.